Heliyon 10 (2024) e24244

Contents lists available at ScienceDirect

Heliyon

journal homepage: www.cell.com/heliyon

Research article

The prospect of spray pyrolyzed pure, Mn-doped, and Zn-doped nickel oxide thin films as TCO material

M. Esmotara Begum [a], M. Bodiul Islam [a,*], M. Hosne Ara [a], Anannya Doris [a], M. Abdul Kaiyum [a], Md. Rasadujjaman [b]

[a] *Nano Synthesis Laboratory, Department of Glass & Ceramic Engineering, Rajshahi University of Engineering & Technology (RUET), Rajshahi-6204, Bangladesh*

[b] *Department of Physics, Mawlana Bhashani Science and Technology University (MBSTU), Tangail-1902, Bangladesh*

ARTICLE INFO

Keywords:
NiO films
Zn-doped NiO
Mn-doped NiO
Opto-electronic properties

ABSTRACT

Nickel Oxide films with Manganese (Mn) and Zinc (Zn) doping (NiO, $Ni_{1-x}Mn_xO$, and $Ni_{1-x}Zn_xO$; where x = 0, 0.02, 0.04, and 0.06) were fabricated using the spray pyrolysis technique on the glass substrates at 400 °C (673K) temperature. The XRD spectra revealed a polycrystalline nature of the films with cubic crystal structure and a favored growth orientation towards the (111) plane. The SEM micrographs revealed a smooth, homogeneous, and uniform surface, while the EDS spectra confirmed the presence of Ni, O, Zn, and Mn elements in the films. Optical analysis using UV–visible absorption spectroscopy demonstrated high transparency of the films in the visible region (400 nm–900 nm), and the transparency increased with higher Zn doping, reaching ~85 % in $Ni_{0.94}Zn_{0.06}O$ films. Conversely, $Ni_{1-x}Mn_xO$ films show a slight transmission decline with increasing Mn doping concentrations. The sheet resistance of the films was found to be decreased for low-concentration doping and again began to increase for highly doped $Ni_{0.94}Zn_{0.06}O$ and $Ni_{0.94}Mn_{0.06}O$ films. Among all the films, $Ni_{0.98}Zn_{0.02}O$ exhibited the maximum figure of merit, showing the prospect for optoelectronic applications.

1. Introduction

Nickel oxide (NiO), a compound composed of nickel and oxygen atoms, is a prominent material because of its remarkable structural, optical, and electrical characteristics. It showcases p-type semiconducting behavior, having large bandgap energy of 3.6–4 eV [1], which makes it a prospective candidate in electronics. Beyond electronics, NiO has demonstrated its versatility across other fields of applications, including its utilization as electrochromic materials [2], transparent conducting oxides in solar cells [3], a potential application in perovskite solar cells as a hole transport layer [4], exhibited considerable potential in the realm of gas sensing applications [5], a valuable component in photocathodes [6], electrochromic windows [7] and some of other multifaceted role in other contemporary technologies. As a result, many research works have reported focusing on the fabrication routes of NiO thin films with improved structural, morphological, and optical characteristics. Such a diverse array of deposition techniques includes spin coating [8], RF sputtering method [9], chemical spray pyrolysis [10], atomic layer epitaxy [11], sol-gel method, and dip coating method [12]. Very recently, Mo-modified NiO thin film was prepared by the electrodeposition process [13] with excellent electrochemical properties of NiO films that found its suitability as electrode materials in high-performance photocatalytic and supercapacitor devices. All these

* Corresponding author.
E-mail address: mbi@gce.ruet.ac.bd (M.B. Islam).

https://doi.org/10.1016/j.heliyon.2024.e24244
Received 14 September 2023; Received in revised form 18 December 2023; Accepted 4 January 2024
Available online 6 January 2024

techniques have employed to tune the structural, and functional properties of the NiO thin films. Several researchers also worked on evaluating how various deposition parameters of the corresponding techniques affect the structure, morphology and other functional properties of the deposited films. Among all the above-mentioned techniques, the spray pyrolysis method is well known by its uniqueness, safety, simplicity, and cost-effectiveness. Notably, this method enables immediate post-deposition annealing [14] and offers the flexibility to adjust crucial deposition parameters like encompassing substrate temperature [15], precursor solution concentration [10], and film thickness.

It is noteworthy that for device applications, transparent conducting oxides (TCOs) necessitate a delicate balance between transparency and conductivity, i.e., they must have to possess a significant amount of transparency (>80 %) in the visible range of electromagnetic spectra with minimum possible resistivity. However, these two essential parameters are affected inversely with film thickness. On the other hand, the resistivity is around 10^{13} Ωcm of stoichiometric NiO [1], which is quite high and limits its efficiency as transparent conducting oxide in device applications. Thus, having a higher optical transmission of >80 % with the lowest possible resistance is a significant breakthrough in NiO TCOs. Consequently, extensive research has done to enhance the optoelectronic properties of NiO films, paving a promising pathway towards the applications of NiO in optoelectronic devices. Among the efficacious strategies for tailoring the optoelectronic characteristics of NiO thin films, 'doping' with other elements emerges as a fruitful method. Several studies have investigated the influence of a variety of doping elements including Lithium (Li) [16], Magnesium (Mg) [17], Aluminum (Al) [18], Potassium (K) [19], as metallic elements, Manganese (Mn) [20], Cobalt (Co) [21], Copper (Cu) [22], Zinc (Zn) [23,24] as transition metals, Gallium (Ga) [18], Yttrium (Y) [25], Cadmium (Cd) [26], Indium (In) [18,27], Lanthanum (La) [28], Ruthenium (Ru) [29] and some of the others that can induce changes in the band structure, affecting the electrical conductivity, optical transmittance and catalytic activity of the NiO films. Recently, a group of researchers has fabricated rare earth elements: Praseodymium (Pr), Terbium (Tr), and Erbium (Er) doped NiO films [30] that showed excellent ultraviolet photosensitivity suited for the application of photodetectors. Thus, applications of NiO films is progressively expanding across multidisciplinary fields. Consequently, research on NiO films are being actively ongoing to enhance the properties of NiO films and unlock new possibilities [31–33]. However, the authors of this present work aim to fabricate NiO films adopting a simple, inexpensive, and homemade spray pyrolysis technique with the addition of Manganese (Mn) and Zinc (Zn) as dopant elements. Manganese (Mn) and Zinc (Zn) are prominent transition metals having an oxidation state of +2, the same valence as Nickel (Ni), and also possess quite close ionic radii, Mn^{2+} (0.83 Å), Zn^{2+} (0.74 Å), and Ni^{2+} (0.69 Å) [34]. Therefore, it is expected that the incorporation of Zn^{2+} and Mn^{2+} ions will easily substitute Ni^{2+} ions and take position into the host lattice without any significant changes in the crystalline structure of NiO. Authors of this work thus motivated to synthesize NiO, $Ni_{1-x}Zn_xO$, and $Ni_{1-x}Mn_xO$ (where x = 0, 0.02, 0.04, and 0.06 respectively) films to investigate the effects of Zn-doping and Mn-doping on the crystalline structure, surface morphology, and optoelectronic properties of NiO films. A spray pyrolysis technique, with a self-developed lab setup, was used to prepare the films, which were then subjected to various characterization techniques to evaluate the effects of doping on the properties of the films as a prospect for optoelectronic applications.

2. Materials and methodology

Nickel Oxide (NiO) thin films, with Zinc (Zn) and Manganese (Mn) doping, were fabricated by using the chemical spray pyrolysis method. Nickel acetate tetra-hydrate ($Ni(CH_3COO)_2.4H_2O$) salt was used as the precursor for NiO host materials. Zinc acetate dihydrate ($Zn(CH_3COO)_2.2H_2O$) salt was used as a source of Zinc (Zn) ions and manganese acetate tetra-hydrate ($Mn(CH_3COO)_2.4H_2O$) salt was used as the dopant source for Mn. Deionized distilled water was used as solvent materials for preparing the salt solutions. Microscopic glass slides were used as substrate materials on which the films were deposited.

Precursor solutions preparation was started by weighing the required grams of precursor salt into a beaker. Then the solvent was measured by a measuring cylinder and added to the beaker with the salt. For homogeneous mixing and desolation of the salt, the entire mixture was stirred for about 20 min using a magnetic stirrer. The concentration of the solution was kept 0.1 M. By adopting this process, both the host and dopant precursor solutions were prepared separately and preserved for use. Before deposition, glass substrates were cleaned, dried, and preserved in an airtight container. Cleaning of the substrates was performed by treating them with diluted ethanol, followed by ringing with distilled water.

To prepare the pure NiO films, the precursor solution of nickel acetate tetra-hydrate was sprayed over the preheated glass substrate. The temperature of the substrate was ~400 °C. The distance of the nozzle from the glass substrate were around 25 cm, and the rate of spraying precursor was 2 mL/min while maintaining 1.5 bar gas pressure. When the solution is sprayed as tiny droplets towards the heated substrate, they decomposed, and the reaction products adhere to the substrate by the action of heat of the substrate. The following reaction took place over the substrate.

$$Ni(CH_3COO)_2.4H_2O \rightarrow NiO + CO_2\uparrow + CH_4\uparrow + \text{Steam}\uparrow$$

After completion of the deposition process, the samples were cooled to room temperature, collected, and delivered to different characterizations and testing units for further evaluation.

To prepare the $Ni_{1-x}Mn_xO$ and $Ni_{1-x}Zn_xO$ samples, the required amount of host solution (2 %, 4 %, and 6 %) were replaced by Mn and Zn solutions, respectively. Then the entire solution was stirred for about 20 min for the intimate mixing. The doped films were then prepared following the above-mentioned process. The following reactions took place over the substrates for Mn and Zn doped samples.

$$Ni(CH_3COO)_2.4H_2O + Mn(CH_3COO)_2.4H_2O \rightarrow Ni_{1-x}Mn_xO + CO_2\uparrow + CH_4\uparrow + \text{Steam}\uparrow$$

$$Ni(CH_3COO)_2.4H_2O + Zn(CH_3COO)_2.2H_2O \rightarrow Ni_{1-x}Zn_xO + CO_2\uparrow + CH_4\uparrow + \text{Steam}\uparrow$$

All the prepared samples were characterized by several characterization techniques. The thickness of the films were measured by using Newton's Ring Method. Films with uniform thickness were accounted for further processing. The thickness of the films were ~200 nm for both doped and undoped samples. The basic structural characteristics of the films were studied by using the X-ray Diffraction (XRD) technique with Cu Kα radiation (LabX XRD-6100, Shimadzu, Japan). Surface morphology with elemental information was characterized using Scanning Electron Microscope (SEM) along with Energy dispersive spectroscopy (EDS) (ZEISS-EVO 18). The optical characteristics were observed using a double beam spectrophotometer (UV–1601PC Shimadzu, Japan) in between 300 nm and 900 nm wavelength range. Keithley 6517B Electrometer was used to determine the resistivity of the specimens.

3. Results and discussion

3.1. Structural analysis

The structural information of the prepared films were investigated using X-ray diffraction (XRD) spectral analysis. XRD patterns of the NiO, $Ni_{1-x}Zn_xO$, and $Ni_{1-x}Mn_xO$ (where x = 0, 0.02, 0.04, and 0.06) films are depicted in Figs. 1 and 2, respectively. These XRD spectra were further analyzed to obtain comprehensive insights into the crystalline behavior of the films, such as crystal structure, crystallite sizes, and lattice parameters.

The prepared films mostly showed a crystalline nature with a cubic crystal structure evident from ICSD-024014 data [Reference code: 01-073-1519] having well-defined peaks indexed as (111), (200), and (222) planes. No other peaks corresponding to precursor impurities, such as Ni, Zn, or Mn metals, and their compounds were evident at the resolution limit of the characterization apparatus. It indicates that doping elements have successfully substituted in the NiO host lattice.

As observed in Figs. 1 and 2, the intensity of the peak corresponding to the (111) plane found to be higher than the other reflection planes (200) and (222), which indicates the preferential growth orientation of the films along the (111) plane. The incorporation of Zn and Mn dopants in NiO films has a pronounced influence on their crystalline behavior, which is clearly identified in the corresponding spectral analysis. With increasing Zn-doping in the host lattice, the intensity of the major peak (111) grows sharply, which indicates favorable formation of crystallites with Zn doping. But the peak position slightly shifted to lower angles. This observation seems to be caused by the lattice expansion due to the substitution of comparatively smaller sized Ni ions (ionic radius 0.69 Å) by larger sized Zn (ionic radius 0.74 Å) ions. A Similar effect also reported for Cd doped NiO films (where the ionic radius of Cd was 0.97 Å larger than Ni ion) [26]. Furthermore, this is also well matched with d-spacing values, which were calculated using equation (1), and all the values are listed in Table 1. Moreover, it is observed that incorporation of Zn ion into the structure of NiO films can favorably increase the crystallization behavior resulting in the increase of peak intensity than pristine NiO films. It demonstrates that Zn doping can facilitate the nucleation site during film formation and provide a favorable environment for crystalline growth. This leads to the formation of larger and more ordered crystallites, thereby increasing crystallinity.

Conversely, the substitution of Mn doping gradually declines the crystalline behavior of the films evidenced in Fig. 2. With increasing Mn concentrations in $Ni_{1-x}Mn_xO$ films (where x = 0, 0.02, 0.04, and 0.06), the intensity of the peaks begin to drop and

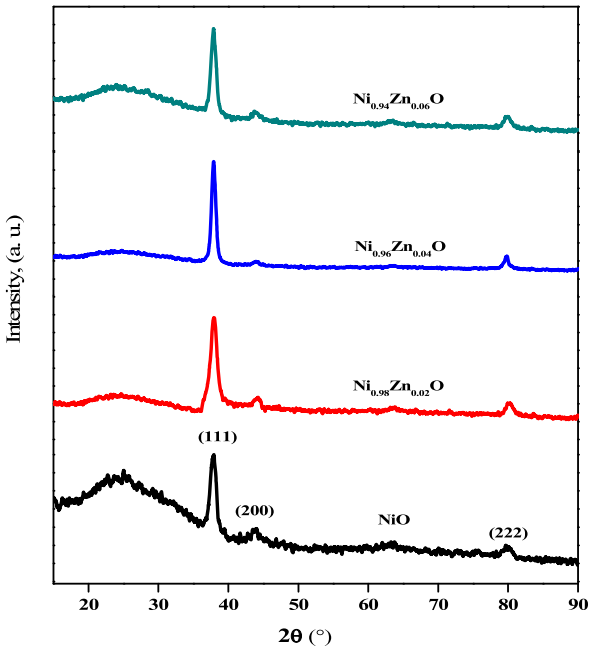

Fig. 1. XRD graph for $Ni_{1-x}Zn_xO$ films (where x = 0, 0.02, 0.04, and 0.06).

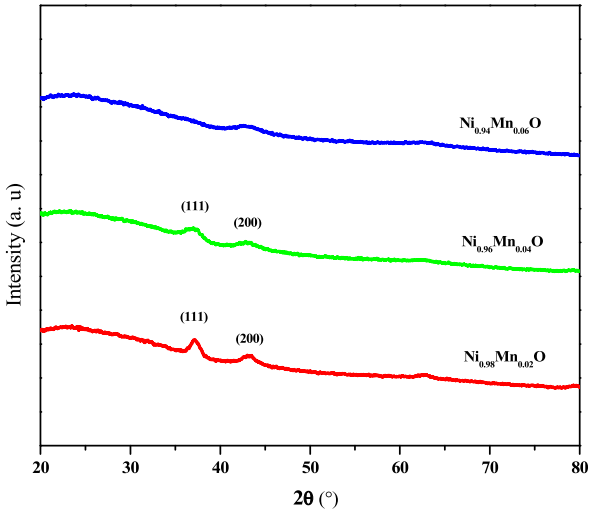

Fig. 2. XRD graph for $Ni_{1-x}Mn_xO$ films (where x = 0, 0.02, 0.04, and 0.06).

Table 1
Various structural parameters for pure NiO, $Ni_{1-x}Zn_xO$, and $Ni_{1-x}Mn_xO$ films.

Doping Concentrations		Peak Position (2θ) (°)	FWHM (°)	d-spacing (Å)	Crystallite Size (D)	Lattice Constant a, (Å)
Pure NiO Films		37.91	0.93198	2.371	14.95 nm	4.106
Zn	0.02 Zn	37.89	0.88023	2.372	15.82 nm	4.108
	0.04 Zn	37.87	0.75357	2.374	18.46 nm	4.111
	0.06 Zn	37.86	0.95288	2.374	14.59 nm	4.111
Mn	0.02 Mn	37.24	1.37546	2.412	06.37 nm	4.179
	0.04 Mn	37.13	1.98324	2.419	04.41 nm	4.191
	0.06 Mn	–	–	–	–	–

eventually declines at case x = 0.06 doping concentration. The position of the dominant peak again slightly shifted to lower angles, which can be attributed to lattice expansion due to the substitution of comparatively smaller-sized Ni ion (ionic radius 0.69 Å) by larger-sized Mn (ionic radius 0.83 Å) ions and also well-matched with d-spacing values. Moreover, it is observed that Mn doping deteriorates the crystalline behavior of the NiO films, which can be attributed to the deformation of the NiO lattice induced by the higher amount of stress generation caused by the size difference between host ions and dopants. This possibly leads to the formation of secondary phases or segregation of dopants into the regions of grain boundaries, but quantity is too small to detect in the resolution limit of the characterization apparatus. The d-spacing and lattice constant values were calculated using the following equations (1) and (2), respectively.

$$2d_{hkl}\ sin\ \theta = n\lambda \tag{1}$$

$$d_{hkl} = \frac{a}{\sqrt{h^2 + k^2 + l^2}} \tag{2}$$

Where n indicates as the degree of order of diffraction (usually n = 1); λ represents the wavelength of the incident X-ray. Table 1 in the following lists all the calculated values. The d-spacing (2.371 Å to 2.419 Å) and lattice constant (4.106 Å to 4.191 Å) values both slightly increase with increasing doping percentages. This incremental effect may be attributed to the substitution of smaller host Ni ions by larger sized Zn and Mn dopant ions. These results are also consistent with previously reported data. A group of researchers reported that La doping up to 4 % can increase d-spacing and lattice constant values to 2.411 Å and 4.176 Å, respectively, which is comparable to present literature [28].

The crystallite size (D) of the deposited films was estimated using Scherer's formula as follows [35].

$$D = \frac{k\lambda}{\beta\ cos\ \theta} \tag{3}$$

Where λ represents the wavelength of the incident X-ray, θ is the position of the Bragg diffraction peaks (in radians), and β is defined as the full width at half maximum (FWHM) of the corresponding diffraction peaks. All these calculated values are listed in Table 1. The crystallite size of the NiO films was 14.95 nm, which was found to be increased at 15.82 nm and 18.46 nm for $Ni_{0.98}Zn_{0.02}O$ and $Ni_{0.96}Zn_{0.04}O$ films respectively. On the other hand, the value was found to be lowered again at 14.59 nm for $Ni_{0.94}Zn_{0.06}O$ films. This

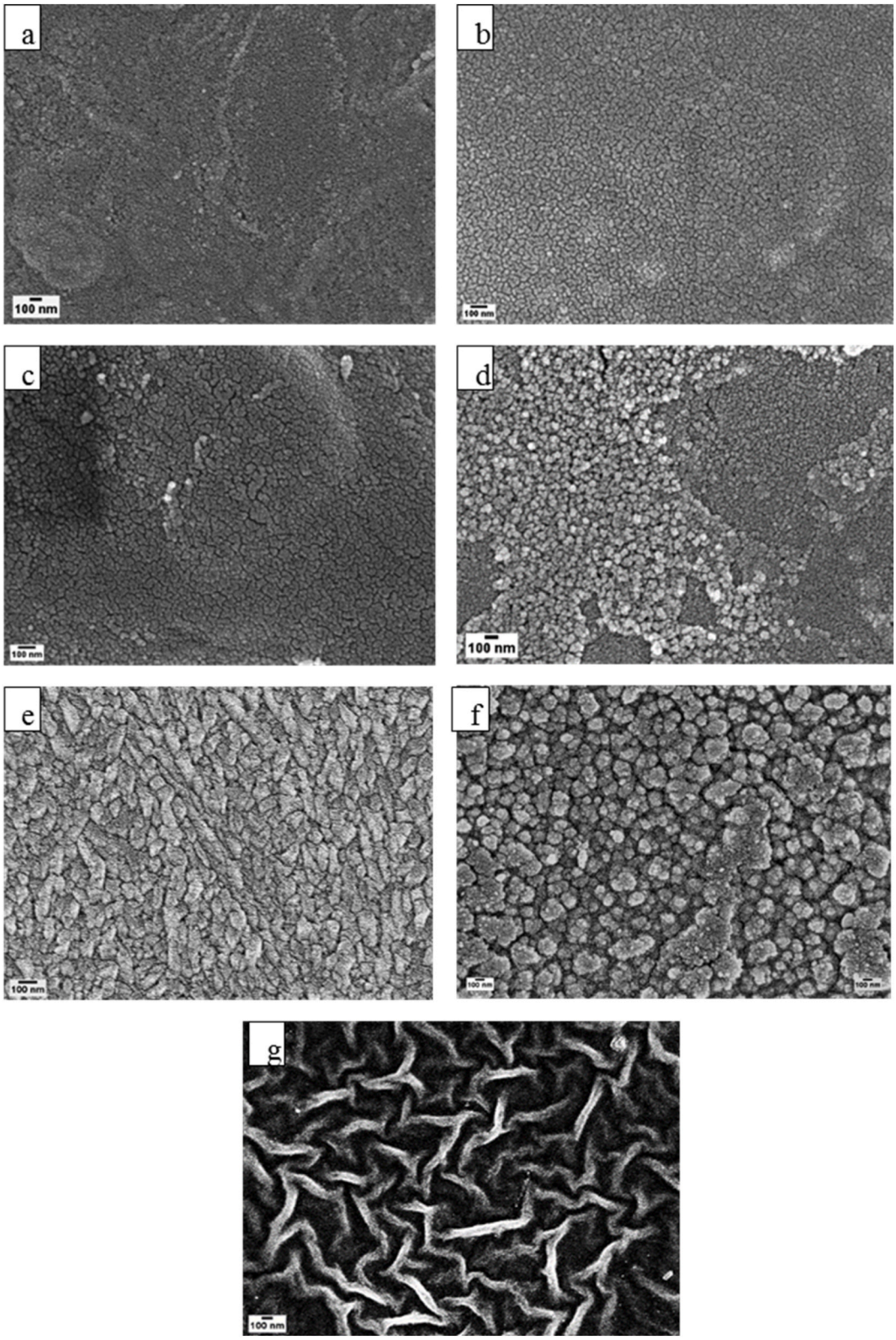

Fig. 3. SEM micrographs of Zn and Mn-doped NiO films; a) NiO, b) $Ni_{0.98}Zn_{0.02}O$, c) $Ni_{0.96}Zn_{0.04}O$, d) $Ni_{0.94}Zn_{0.06}O$, e) $Ni_{0.98}Mn_{0.02}O$, and f) $Ni_{0.96}Mn_{0.04}O$ g) $Ni_{0.94}Mn_{0.06}O$.

observation is attributed to the slight increment of lattice parameters of the crystals and favorable nucleation and growth conditions. Further, the slightly higher atomic radius of the dopant Zn^{2+} ions compared to the host Ni^{2+} ions may also attribute to the increment of crystallite size. In the case of high doping concentrations, a slight decrease in crystallite sizes is due to the dragging force by the excess amount of dopant on boundary motion, resulting in reduced growth kinetics of the NiO films. On the other hand, with increasing concentrations of Mn doping into NiO lattices, very small crystallites were observed up to 4 % Mn doping. These insights were possibly the reason for the degradation of the crystalline quality of the $Ni_{1-x}Mn_xO$ films. This decrement in crystalline behavior also observed in a literature analyzing sol-gel spin-coated Mn-doped NiO thin films where the crystallite size of the NiO films decreased from 19.86 nm to 12.11 nm [20].

3.2. Morphology and Compositional analysis

To observe the surface morphology along with the chemical composition of the NiO, $Ni_{1-x}Zn_xO$, and $Ni_{1-x}Mn_xO$ (where x = 0, 0.02, 0.04, and 0.06 respectively) films, Scanning Electron Microscopy measurement along with EDS analysis were performed. Fig. 3(a)-(d) shows the 2D SEM images of Zn-doped NiO films. The SEM micrographs of the NiO films reveal the presence of very fine nanograins

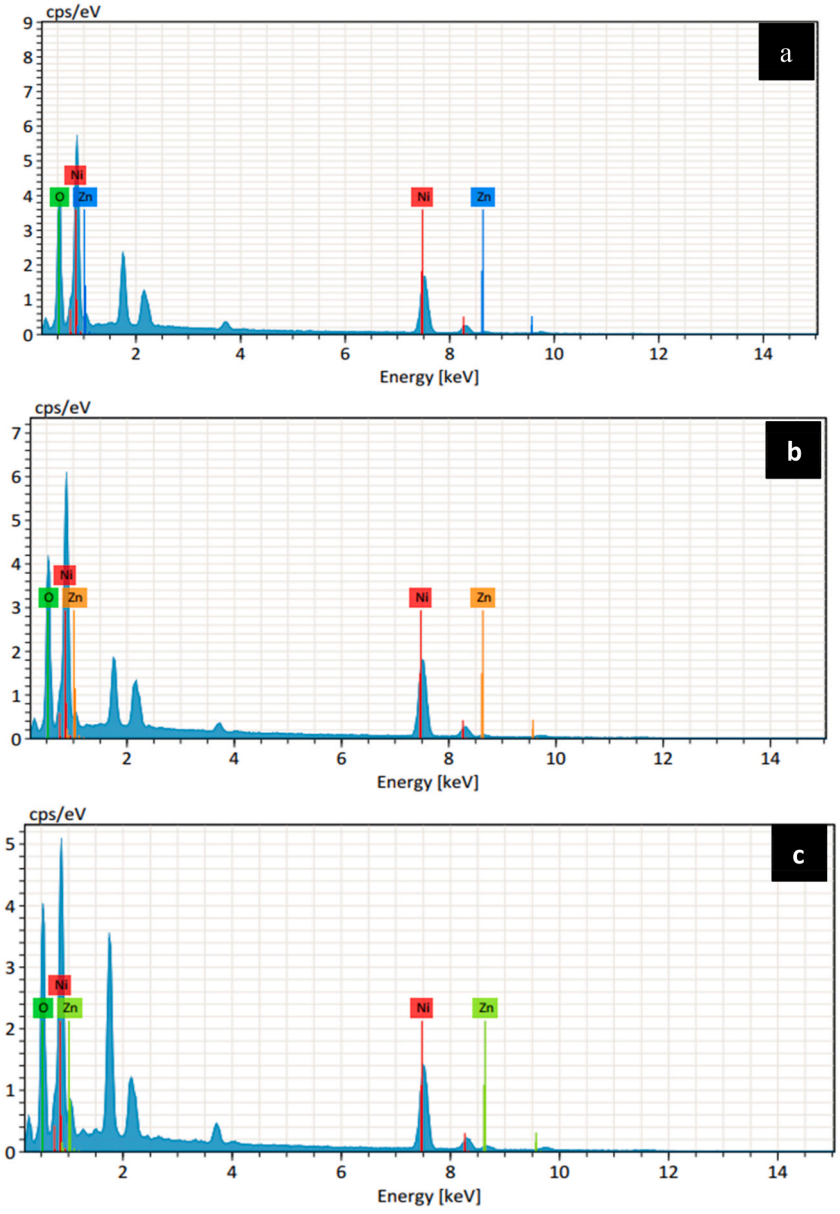

Fig. 4. EDS spectra of Zn doped NiO films; a) $Ni_{0.98}Zn_{0.02}O$, b) Ni0.96Zn0.04O, and c) $Ni_{0.94}Zn_{0.06}O$.

uniformly distributed across the film's surface. This kind of surface morphology also observed for K-doped NiO thin films which were prepared by rapid pyrolysis of the sol-gel method [36]. The surface morphology of the NiO thin films appears remarkably smooth and uniform, devoid of notable surface irregularities like pores or cracks. Furthermore, the introduction of Zn can alter the grain size and surface roughness of the pristine NiO films.

With the increasing Zn concentration, the surface becomes smoother with distinguishable grain boundaries for $Ni_{0.98}Zn_{0.02}O$ and $Ni_{0.96}Zn_{0.04}O$ films. With further increasing of Zn concentration, for $Ni_{0.94}Zn_{0.06}O$ films the incremental grain size observed along with some loose granular regions. However, the addition of Zn can act as a grain growth promoter that inherently improves the crystal quality, evidenced by XRD analysis results in coarser grains in doped films. On the other hand, the effect of Mn doping also has a notable effect on the morphology of the NiO films shown in Fig. 3 (e), (f), and (g). With the substitution of 2 % Mn and 4 % Mn in NiO films ($Ni_{0.98}Mn_{0.02}O$ and $Ni_{0.96}Mn_{0.04}O$ films), the grains became elongated, and the grain boundaries more pronounced. In the case of 6 % Mn doping ($Ni_{0.94}Zn_{0.06}O$ film), the morphology has developed a distinguishable feature. As depicted in Fig. 3, the grains began to elongate for 2 % Mn doping, and some irregular fiber-like streaks observed for 6 % Mn doping. Distinguished features of surface morphology also reported by several other researchers. Potassium (K) [19] and Ruthenium (Ru) [29] doping can reduce the roughness values of NiO films that prepared by spray pyrolysis techniques.

The elemental composition of the prepared films was investigated via Energy Dispersive Spectroscopic Analysis (EDS). Fig. 4(a–c) shows spectra of $Ni_{1-x}Zn_xO$ (where x = 0.02, 0.04, and 0.06) films, and Fig. 5 (a) and (b) shows spectra of $Ni_{1-x}Mn_xO$ (where x = 0.02 and 0.06). All these EDS spectra confirm the presence of Zn, Mn, Ni, and O atoms in the deposited films, and no other impurities evidenced.

3.3. Optical properties

The optical properties of the NiO, $Ni_{1-x}Mn_xO$, and $Ni_{1-x}Zn_xO$ films were examined by UV–visible (UV–Vis) transmission-absorbance measurements. The UV–vis transmission spectra of NiO films with different Mn and Zn concentrations in the region of electromagnetic wavelengths spanning from 300 nm to 900 nm (encompassing the UV–visible and also near IR region) are depicted in Fig. 6 (a) and Fig. 6 (b) respectively. These spectra demonstrate that the produced films exhibit a high transparency, with an apparent transparency in the visible region of roughly 80 %. In the region 300 nm–340 nm, minimum transmittance observed due to the strong absorption region resulting from electronic transition shown in Fig. 7 (a) and (b). Fig. 6 (a) depicts that with increasing Zn doping concentrations in $Ni_{1-x}Zn_xO$ films, transparency of the films was almost similar but slightly increased in the visible region. But the absorption edge was almost stable as pristine NiO films which can be attributed to the quite closed electronic configuration of Ni and Zn ions. Thus increased transparency of the doped films can be attributed to the improved crystal quality of the films well matched with XRD and SEM. This improved optical transparency of the NiO films was also previously reported [37,38].

Conversely, the addition of Mn in $Ni_{1-x}Mn_xO$ films slightly lowers the transparency and widens the absorption edges shown in Figs. 6 (b) and Fig. 7 (b). This can be attributed to the degradation of crystal quality and increased defect populations that lead to the formation of new energy states below or near the bandgap. These energy levels facilitate electronic transitions that result in increased

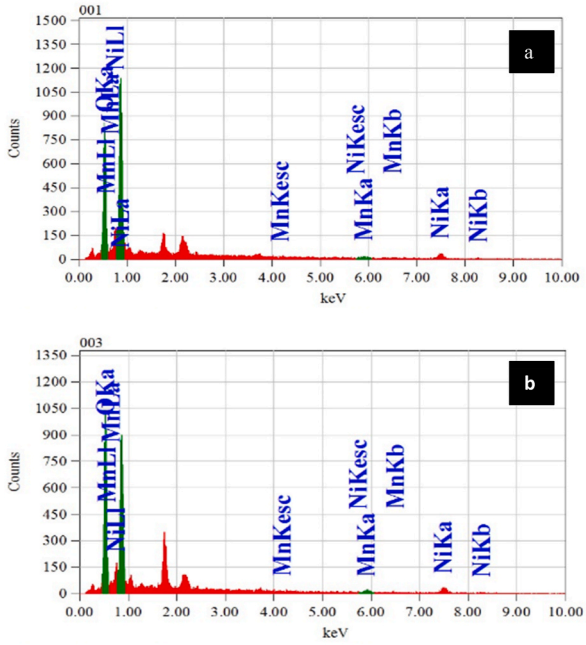

Fig. 5. EDS spectra of Mn-doped NiO films; a) $Ni_{0.98}Mn_{0.02}O$ and b) $Ni_{0.94}Mn_{0.06}O$.

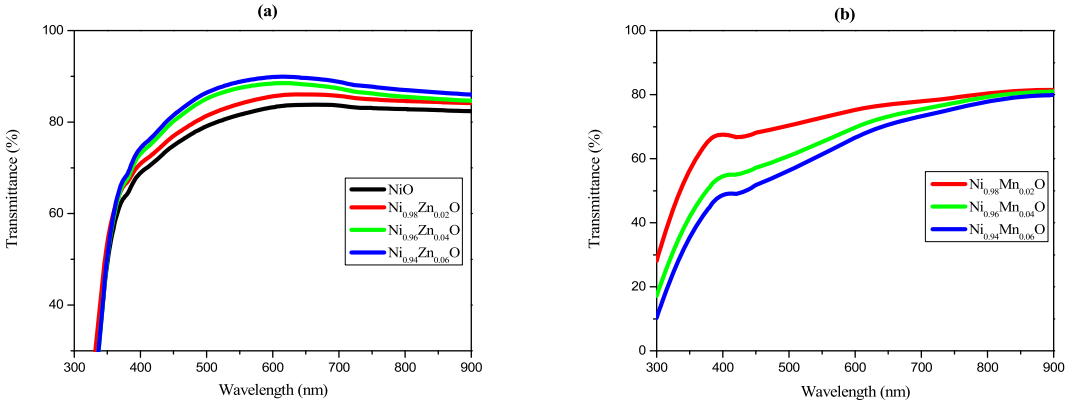

Fig. 6. Transmission spectra of the as-deposited NiO films; a) $Ni_{1-x}Zn_xO$ and b) $Ni_{1-x}Mn_xO$ (where x = 0, 0.02, 0.04, and 0.06).

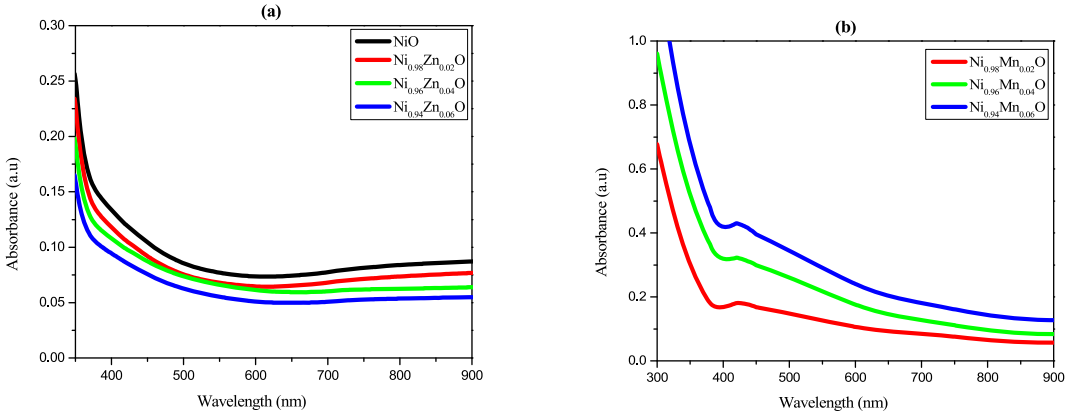

Fig. 7. Absorption spectra of the as-deposited NiO films; a) $Ni_{1-x}Zn_xO$ and b) $Ni_{1-x}Mn_xO$ (where x = 0, 0.02, 0.04, and 0.06).

absorption of light. Consequently, the overall transmittance of the films diminishes as the Mn doping concentration rises. This type of effect also evidenced in La-doped NiO thin films, which also prepared using the spray pyrolysis technique [28]. Substitutional doping with Cu ion in NiO films also reduces transmission values of the films reported by several other researchers [39,40].

The band gap energy, Eg, of the prepared samples, was calculated using Tauc plot. As shown in Fig. 8 (a) and (b), the values of $(\alpha h\upsilon)^2$ were plotted on the y-axis, while the values of photon energy, hυ were plotted on the x-axis. Eg values were estimated by extrapolating the linear portion of the plotted curves into the x-axis. Following is the equation for Tauc's plot [41]:

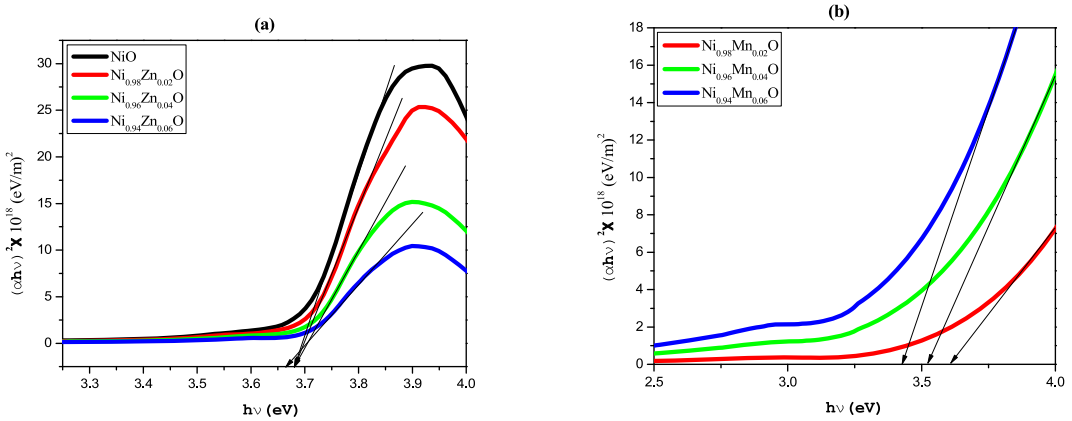

Fig. 8. Tauc's Plot for NiO films; a) $Ni_{1-x}Zn_xO$ and b) $Ni_{1-x}Mn_xO$ (where x = 0, 0.02, 0.04, and 0.06).

$$\alpha h\upsilon = A(h\upsilon - Eg)^n \quad (4)$$

Where n denotes the number 2 or ½. Generally, 1/2 is counted for the materials that have direct bandgap, and 2 is accounted for the materials that have indirect bandgap, α is denoted as the absorption coefficient of the films, A is defined as a constant that depends on photon energy, h is for Planck's constant, υ represents the frequency of the incident photon that is directed towards the sample. By drawing a curve $(\alpha h\upsilon)^2$ versus $(h\upsilon)$, the optical band gap energy of the undoped NiO films and also the Zn doped and Mn doped films were estimated as shown in Fig. 8 (a) and (b) for $Ni_{1-x}Zn_xO$ and $Ni_{1-x}Mn_xO$ films respectively, and listed in Table 2. As listed in Table 2, the calculated Eg value for the pure NiO thin film was 3.66 eV and remains quite stable for $Ni_{1-x}Zn_xO$ films. This type of high band gap value was also observed for Mg-doped NiO films and increased from 3.56 eV to 3.62 eV for higher concentrations of doping [17]. On the other hand, increasing Mn doping concentration lowers the values progressively from 3.66 eV to 3.43 eV for up to 6 % Mn doping. The reported Eg values thus indicate that the constructed samples could be used in photovoltaic applications.

The extinction coefficient is a property of a species that determines how strongly it absorbs or reflects radiation or light at a specific wavelength. Extinction coefficients were calculated using optical experimental measurements from the following equation for wavelengths ranging from 350 to 900 nm [42]:

$$k = \frac{\alpha\lambda}{4\pi} \quad (5)$$

Where k, λ, and α are the extinction coefficient, the wavelength, and the absorption coefficient, respectively.

Fig. 9 (a) and (b) exhibit k values as a function of photon energy for $Ni_{1-x}Zn_xO$ and $Ni_{1-x}Mn_xO$ films, respectively. The corresponding k values at wavelength 400 nm (3.1 eV) of the $Ni_{1-x}Zn_xO$ films are 0.0493, 0.0425, 0.0395, and 0.0349 for x = 0.02, 0.04, 0.06 respectively. It demonstrates that the extinction coefficient value gradually declines with the increasing concentration of Zn doping. These lower values of k are also indicative of having films with high optical transparency along with enhanced surface homogeneity.

3.4. Electrical characteristics

To evaluate the electrical properties, sheet resistance of the deposited NiO, $Ni_{1-x}Zn_xO$, and $Ni_{1-x}Mn_xO$ (where x = 0, 0.02, 0.04, and 0.06 respectively) films were measured by four-point probe method at room temperature, and the resultant values are listed in Table 3. The resistivity values of the films were quite high (in the order of 10^3 Ωcm) shown in Fig. 10. In case of doped films, the resistivity begins to drop first and then increases for higher doping percentage. It is worth noting that the conduction phenomenon of NiO films is attributed to the presence of a non-stoichiometric NiO structure, which contains Ni^{3+} ions within their structure, leading to the formation of vacant sites. These vacancies facilitate conduction behavior in NiO by hole mobility. However, when Zn^{2+} and Mn^{2+} ions are introduced as dopants in higher concentrations, they probably occupy these vacant sites. This observation can reduce the carrier concentration within the material, leading to a decrease in conductivity.

3.5. FOM

To assess the suitability of the deposited films as a TCO material in optoelectronic applications, the figure of merit (FOM) of $Ni_{1-x}Zn_xO$ and $Ni_{1-x}Mn_xO$ films was calculated using Haacke's equation [43].

$$FOM = \frac{T^x}{R_s} \quad (6)$$

Where T is the transmission, x = 10, and R_s is the sheet resistance. The calculated FOM values are listed in Table 3. With the incorporation of Zn ion in the structure of NiO, the FOM values increase slightly. The maximum FOM was observed for $Ni_{0.98}Zn0_{.02}O$ and $Ni_{0.96}Zn0_{.04}O$ compositions. With increasing Mn concentrations, FOM values began to drop, and the minimum was for $Ni_{0.94}Mn0_{.06}O$ composition. These findings attributed to the higher level of resistivity of the samples. This kind of high resistivity value also reported by several other researchers, one of them for La-doped NiO films [28]. All the findings are summarized graphically in Fig. 11.

4. Conclusions

Nickel Oxide films with Manganese (Mn) and Zinc (Zn) doping have been fabricated successfully using a homemade chemical spray pyrolysis thin films deposition technique onto glass substrates. XRD analyses confirmed the crystalline nature of the prepared films and the preferential growth orientation of the films along (111) plane directions. The surface morphology of the films was found to be smooth, containing nanoscale grains uniform and homogeneously distributed, and devoid of any cracks and defects. The incorporation of Zn and Mn ions as dopants, yields a notable effect on the optoelectronic properties of the NiO films. With increasing Zn doping concentrations from 2 % to 6 %, transparency of the films increases slightly from 82 % to 88 % in the visible light region (400 nm–900 nm). On the other hand, the addition of Mn ions lowers the transparency of the NiO films. The sheet resistance value of the doped films decreases for low doping concentrations (2 %–4%) and again begins to increase for higher doping concentrations. As a result, the figure of merit value of the films was found to be increased for Zn-doped films. Among all the films, $Ni_{0.96}Zn_{0.04}O$ and $Ni_{0.98}Zn_{0.02}O$ films show the maximum figure of merit emerging applicability of the films in optoelectronic applications.

Table 2
Band gap and extinction coefficient values for pure NiO, $Ni_{1-x}Zn_xO$, and $Ni_{1-x}Mn_xO$ films.

Doping Concentrations		Band Gap, Eg (eV)	Extinction coefficient, k
Pure NiO Films		3.66	0.0493
Zn	0.02	3.67	0.0425
	0.04	3.67	0.0395
	0.06	3.67	0.0349
Mn	0.02	3.61	0.0643
	0.04	3.52	0.1155
	0.06	3.43	0.1536

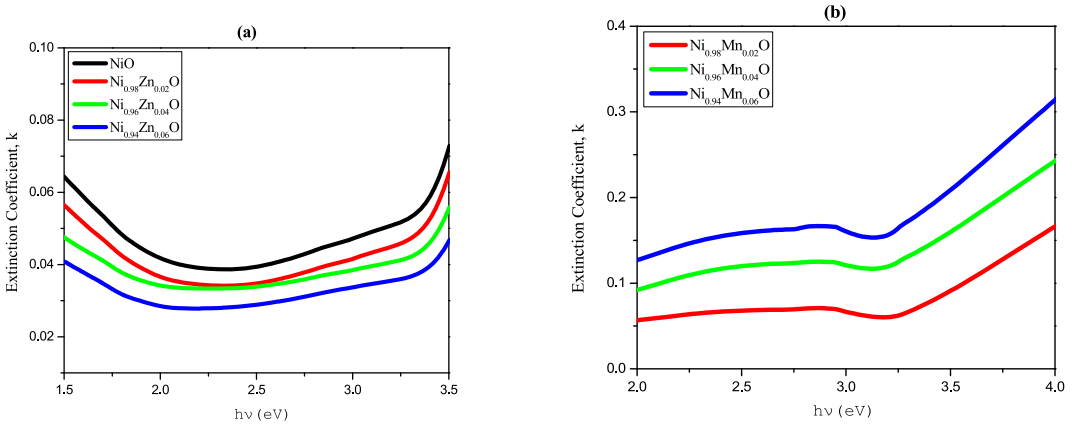

Fig. 9. Extinction coefficient of NiO films; a) $Ni_{1-x}Zn_xO$ and b) $Ni_{1-x}Mn_xO$ (where x = 0, 0.02, 0.04, and 0.06).

Table 3
Various optoelectronic parameters for pure NiO, $Ni_{1-x}Zn_xO$, and $Ni_{1-x}Mn_xO$ films.

Doping concentrations		Transmission, T	Sheet Resistance, R_s ($\times 10^6$ Ω)	Resistivity, ρ ($\times 10^3$ Ωcm)	FOM ($\times 10^{-6}$ Ω^{-1})
Pure NiO		0.82	93.3	2.8	0.00147
Zn	0.02	0.84	39.7	1.19	0.00441
	0.04	0.87	82.6	2.48	0.00310
	0.06	0.88	113.3	3.45	0.00245
Mn	0.02	0.73	87.7	2.63	0.00049
	0.04	0.65	126.3	3.79	0.00011
	0.06	0.61	148.3	4.45	0.00005

Data Availability

Data will be made available on reasonable request.

Additional information

No additional information is available for this paper.

CRediT authorship contribution statement

M. Esmotara Begum: Writing - original draft, Methodology, Formal analysis. **M. Bodiul Islam:** Writing - review & editing, Supervision, Conceptualization. **M. Hosne Ara:** Methodology. **Anannya Doris:** Methodology. **M. Abdul Kaiyum:** Writing - original draft, Formal analysis. **Md. Rasadujjaman:** Formal analysis, Data curation.

Declaration of competing interest

The authors declare that they have no known competing financial interests or personal relationships that could have appeared to influence the work reported in this paper.

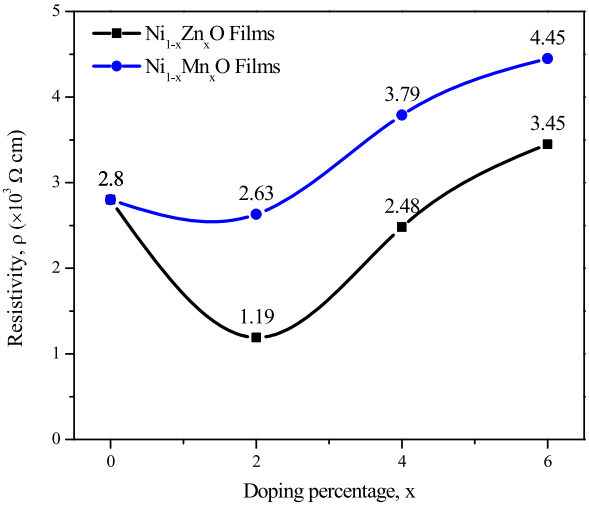

Fig. 10. Electrical Resistivity of $Ni_{1-x}Zn_xO$ and $Ni_{1-x}Mn_xO$ (where x = 0, 0.02, 0.04, and 0.06).

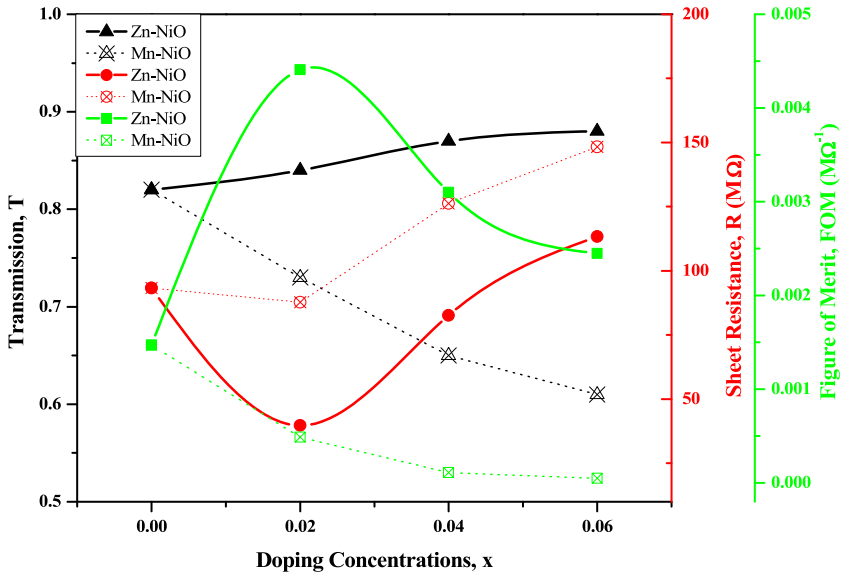

Fig. 11. Opto-electric Characteristics of the $Ni_{1-x}Zn_xO$ and $Ni_{1-x}Mn_xO$ (where x = 0, 0.02, 0.04, and 0.06).

Acknowledgments

The authors would like to express gratefulness to the Glass & Ceramic Engineering Department, Rajshahi University of Engineering & Technology (RUET), Bangladesh, for their support in accomplishing this work.

References

[1] D. Adler, J. Feinleib, Electrical and optical properties of narrow-band materials, Phys. Rev. B 2 (1970) 3112–3134, https://doi.org/10.1103/PhysRevB.2.3112.
[2] S.H. Lin, F.R. Chen, J.J. Kai, Electrochromic properties of nano-structured nickel oxide thin film prepared by spray pyrolysis method, Appl. Surf. Sci. 254 (2008) 2017–2022, https://doi.org/10.1016/j.apsusc.2007.08.029.
[3] H. Sato, T. Minami, S. Takata, T. Yamada, Transparent conducting p-type NiO thin films prepared by magnetron sputtering, Thin Solid Films 236 (1993) 27–31, https://doi.org/10.1016/0040-6090(93)90636-4.
[4] M.B. Islam, M. Yanagida, Y. Shirai, Y. Nabetani, K. Miyano, NiOx hole transport layer for perovskite solar cells with improved Stability and reproducibility, ACS Omega 2 (2017) 2291–2299, https://doi.org/10.1021/acsomega.7b00538.
[5] C. Lee, C. Chiang, Y. Wang, R. Ma, A self-heating gas sensor with integrated NiO thin-film for formaldehyde detection 122 (2007) 503–510, https://doi.org/10.1016/j.snb.2006.06.018.
[6] F. Vera, R. Schrebler, E. Muñoz, C. Suarez, P. Cury, H. Gómez, R. Córdova, R.E. Marotti, E.A. Dalchiele, Preparation and characterization of Eosin B- and Erythrosin J-sensitized nanostructured NiO thin film photocathodes, Thin Solid Films 490 (2005) 182–188, https://doi.org/10.1016/j.tsf.2005.04.052.
[7] H. Huang, J. Tian, W.K. Zhang, Y.P. Gan, X.Y. Tao, X.H. Xia, J.P. Tu, Electrochim. Acta 56 (2011) 4281–4286, https://doi.org/10.1016/j.electacta.2011.01.078.

[8] B.T. Raut, S.G. Pawar, M.A. Chougule, S. Sen, V.B. Patil, New process for synthesis of nickel oxide thin films and their characterization, J. Alloys Compd. 509 (2011) 9065–9070, https://doi.org/10.1016/j.jallcom.2011.06.029.

[9] H.L. Chen, Y.M. Lu, W.S. Hwang, Characterization of sputtered NiO thin films, Surf. Coatings Technol. 198 (2005) 138–142, https://doi.org/10.1016/j.surfcoat.2004.10.032.

[10] B.A. Reguig, M. Regragui, M. Morsli, A. Khelil, M. Addou, J.C. Bernède, Effect of the precursor solution concentration on the NiO thin film properties deposited by spray pyrolysis, Sol. Energy Mater. Sol. Cells 90 (2006) 1381–1392, https://doi.org/10.1016/j.solmat.2005.10.003.

[11] M. Utriainen, M. Kro, L. Niinisto, Studies of NiO thin film formation by atomic layer epitaxy 54 (1998) 98–103.

[12] M. Martini, G.E.S. Brito, M.C.A. Fantini, A.F. Craievich, A. Gorenstein, Electrochromic properties of NiO-based thin films prepared by sol-gel and dip coating, Electrochim. Acta 46 (2001) 2275–2279, https://doi.org/10.1016/S0013-4686(01)00396-6.

[13] H.K. Saheed Adewinbi, Vusani Maphiri, R. Marnadu, Mohd Shkir, Njod Mansour Hasan Alsdran, H. Algarni, G. Sujithkumar, Bidini Taleatu, Theophile Niyitanga, Transparent, photosensitive and highly efficient pseudocapacitive binder-free Mo-modified NiO thin film electrode for bifunctional optoelectronic and energy storage applications, J. Alloys Compd. 937 (2023) 168304, https://doi.org/10.1016/j.jallcom.2022.168304.

[14] R. Sharma, A.D. Acharya, S.B. Shrivastava, T. Shripathi, V. Ganesan, Optik Preparation and characterization of transparent NiO thin films deposited by spray pyrolysis technique, Opt. - Int. J. Light Electron Opt. 125 (2014) 6751–6756, https://doi.org/10.1016/j.ijleo.2014.07.104.

[15] M.E. Begum, M.N.A. Chowdhury, M.B. Islam, Results in Materials Structural , morphological and optical characterizations of spray pyrolyzed nickel oxide thin films, Results Mater 14 (2022) 100265, https://doi.org/10.1016/j.rinma.2022.100265.

[16] U.S. Joshi, Y. Matsumoto, K. Itaka, M. Sumiya, H. Koinuma, Combinatorial synthesis of Li-doped NiO thin films and their transparent conducting properties, Appl. Surf. Sci. 252 (2006) 2524–2528, https://doi.org/10.1016/j.apsusc.2005.03.239.

[17] M. Ben Amor, A. Boukhachem, K. Boubaker, M. Amlouk, Structural, optical and electrical studies on Mg-doped NiO thin films for sensitivity applications, Mater. Sci. Semicond. Process. 27 (2014) 994–1006, https://doi.org/10.1016/j.mssp.2014.08.008.

[18] Ha, S.A.I. Loyola Poul Raj, S. Valanarasu, A. Asuntha, R.S. Rimal Isaac, Mohd Shkir, Development of a highly sensitive UV sensor using Al, Ga, and In-doped NiO thin films via nebulizer spray pyrolysis method for photodetector applications, J. Mater. Sci. Mater. Electron. 33 (2022) 11753–11767, https://doi.org/10.1007/s10854-022-08140-w.

[19] A. Loukil, A. Boukhachem, M. Ben Amor, M. Ghamnia, K. Raouadi, Effects of potassium incorporation on the structural, optical, vibrational and electrical properties of NiO sprayed thin films for p-type optical windows, Ceram. Int. 42 (2016) 8274–8289, https://doi.org/10.1016/j.ceramint.2016.02.040.

[20] N.R. Aswathy, JiJi Varghese, Shree Ranjini Nair, R. Vinod Kumar, Structural, optical, and magnetic properties of Mn-doped NiO thin films prepared by sol-gel spin coating, Mater. Chem. Phys. 282 (2022) 125916, https://doi.org/10.1016/j.matchemphys.2022.125916.

[21] R. Sharma, A.D. Acharya, S. Moghe, S.B. Shrivastava, M. Gangrade, T. Shripathi, V. Ganesan, Effect of cobalt doping on microstructural and optical properties of nickel oxide thin films, Mater. Sci. Semicond. Process. 23 (2014) 42–49, https://doi.org/10.1016/j.mssp.2014.02.004.

[22] L. Zhao, G. Su, W. Liu, L. Cao, J. Wang, Z. Dong, M. Song, Optical and electrochemical properties of Cu-doped NiO films prepared by electrochemical deposition, Appl. Surf. Sci. 257 (2011) 3974–3979, https://doi.org/10.1016/j.apsusc.2010.11.160.

[23] T. Sen, A. Biswas, T.K. Rout, R. Thangavel, U.G. Nair, Comparative study of morphological, optical and conductive properties between low and heavily zinc doped nickel oxide thin films as hole transporting material, J. Alloys Compd. 889 (2021) 161613, https://doi.org/10.1016/j.jallcom.2021.161613.

[24] R. Sharma, A.D. Acharya, S.B. Shrivastava, M.M. Patidar, M. Gangrade, T. Shripathi, V. Ganesan, Studies on the structure optical and electrical properties of Zn-doped NiO thin films grown by spray pyrolysis, Opt. - Int. J. Light Electron Opt. (2016) 1–8, https://doi.org/10.1016/j.ijleo.2016.01.050.

[25] Z. Hu, D. Chen, P. Yang, L. Yang, L. Qin, Y. Huang, X. Zhao, Sol-gel-processed yttrium-doped NiO as hole transport layer in inverted perovskite solar cells for enhanced performance, Appl. Surf. Sci. 441 (2018) 258–264, https://doi.org/10.1016/j.apsusc.2018.01.236.

[26] M. Ben Amor, A. Boukhachem, A. Labidi, K. Boubaker, M. Amlouk, Physical investigations on Cd doped NiO thin films along with ethanol sensing at relatively low temperature, J. Alloys Compd. (2016), https://doi.org/10.1016/j.jallcom.2016.09.207.

[27] S. Kerli, U. Alver, H. Yaykaşli, Investigation of the properties of in doped NiO films, Appl. Surf. Sci. (2014) 164–167, https://doi.org/10.1016/j.apsusc.2014.02.141.

[28] C. Mrabet, M. Ben Amor, A. Boukhachem, M. Amlouk, T. Manoubi, Physical properties of La-doped NiO sprayed thin films for optoelectronic and sensor applications, Ceram. Int. 42 (2016) 5963–5978, https://doi.org/10.1016/j.ceramint.2015.12.144.

[29] A. Alshahrie, S. Joudakzis, A.A. Al-Ghamdi, L.M. Bronstein, W.E. Mahmoud, Synthesis and characterization of p-type transparent conducting Ni 1-x Ru x O ($0 \leq x \leq 0.1$) films prepared by pulsed laser deposition, Ceram. Int. 45 (2019) 7984–7994, https://doi.org/10.1016/j.ceramint.2018.09.214.

[30] B.P.I. Loyola Poul Raj, S. Valanarasu, S. Vinoth, N. Chidhambaram, R.S. Rimal Isaac, Mohd Ubaidullah, Shoyebmohamad F. Shaikh, Highly sensitive ultraviolet photodetectors fabricated from rare earth metal ions doped NiO thin films via nebulizer spray pyrolysis method, Sensors Actuators A Phys 333 (2022) 113242, https://doi.org/10.1016/j.sna.2021.113242.

[31] I.L.P. Raj, S. Valanarasu, R. Ade, Y. Bitla, P. Mohanraj, V. Ganesh, I.S. Yahia, Enhancing the ultraviolet photosensing properties of nickel oxide thin films by Zn–La co-doping, Ceram. Int. 48 (2022) 5026–5034, https://doi.org/10.1016/j.ceramint.2021.11.040.

[32] S. Srivastava, C. Dwivedi, A. Yadav, A. Kumar, G. Gupta, P. Singh, Enhanced H2S gas sensing of Pd functionalized NiO thin films deposited by the magnetron sputtering process, Mater. Lett. 351 (2023) 135040, https://doi.org/10.1016/j.matlet.2023.135040.

[33] M. Touati, T. Boucherka, A. Barbadj, N. Brihi, F. Labreche, Low resistivity and transparent Co-doped NiO thin films synthesized by the sol-gel method: structural, morphology and photoluminescence studied for optoelectronic applications, Opt. Mater. 143 (2023) 114235, https://doi.org/10.1016/j.optmat.2023.114235.

[34] R.D. Shannon, Revised effective ionic radii and systematic studies of interatomie distances in halides and chaleogenides, Acta Cryst 32 (1976) 751.

[35] B.D. Cullity, S.R. Stock, Elements of X-Ray Diffraction, third ed., 2014.

[36] N. Wang, C.Q. Liu, C.Q.L.B. Wen, H.L. Wang, S.M. Liu, W.W. Jiang, W.Y. Ding, W.P. Chai, Structural, electrical and optical properties of K-doped NiO films prepared by rapid pyrolysis sol-gel technique, Thin Solid Films 616 (2016) 587–593, https://doi.org/10.1016/j.tsf.2016.08.051.

[37] Y.R. Denny, K. Lee, C. Park, S.K. Oh, H.J. Kang, D.S. Yang, S. Seo, Electronic, electrical and optical properties of undoped and Na-doped NiO thin films, Thin Solid Films 591 (2015) 255–260, https://doi.org/10.1016/j.tsf.2015.04.043.

[38] X. Chen, L. Zhao, Q. Niu, Electrical and optical properties of p-type Li,Cu-codoped NiO thin films, J. Electron. Mater. 41 (2012) 3382–3386, https://doi.org/10.1007/s11664-012-2213-4.

[39] K.H. Kim, C. Takahashi, Y. Abe, M. Kawamura, Effects of Cu doping on nickel oxide thin film prepared by sol-gel solution process, Optik 125 (2014) 2899–2901, https://doi.org/10.1016/j.ijleo.2013.11.074.

[40] S.C. Chen, T.Y. Kuo, Y.C. Lin, H.C. Lin, Preparation and properties of p-type transparent conductive Cu-doped NiO films, Thin Solid Films 519 (2011) 4944–4947, https://doi.org/10.1016/j.tsf.2011.01.058.

[41] N.F. Mott, E.A. Davis, Conduction in non-crystalline systems V. Conductivity, optical absorption and photoconductivity in amorphous semiconductors, Philos. Mag. A 22 (1970) 903–922.

[42] K.O. Ukoba, A.C. Eloka-Eboka, F.L. Inambao, Review of nanostructured NiO thin film deposition using the spray pyrolysis technique, Renew. Sustain. Energy Rev. 82 (2018) 2900–2915, https://doi.org/10.1016/j.rser.2017.10.041.

[43] G. Haacke, New figure of merit for transparent conductors, J. Appl. Phys. 47 (1976) 4086–4089, https://doi.org/10.1063/1.323240.